International Journal of Modern Physics E
© World Scientific Publishing Company

arXiv:1608.08494v2 [nucl-th] 25 Nov 2016

Recent progress on superstrange dynamics

Theodoros Gaitanos
Faculty of Science, School of Physics, Aristotle University of Thessaloniki
55124 Thessaloniki, Greece
tgaitano@auth.gr

Received Day Month Year
Revised Day Month Year

We review the present activities related to hypernuclear production in hadronic in-medium reactions at intermediate energies. The status of theoretical predictions and experimental evidences for the in-medium formation of bound superstrange matter is discussed. Heavy-ion collisions and antiproton-induced reactions at energies close to strangeness production thresholds create the conditions of hypermatter formation. This allows to understand better in-medium hyperon interactions and sets constraints on the strangeness sector of the nuclear equation of state.

Keywords: Hypernuclei, hadron-induced reactions, heavy-ion collisions.

PACS numbers: 25.40.Ve, 25.43.+t, 25.75.Dw, 25.80.Pw, 21.65.Mn, 21.80.+a

1. Introduction

The equation of state (EoS) of strongly interacting matter has been one of the most researched subject in nuclear and hadron physics over the last 50 years. Concrete investigations on the nuclear EoS were initiated in the early 1970s with the realization of the first relativistic nuclear beams at BEVELAC in Berkeley,[1–3] followed by more selective heavy-ion experiments in centrality, particle identification and phase space reconstruction.[4–10] These measurements gave first hints on collective particle flow.[11–15] They allowed first interpretations on the nuclear EoS at different density regions beyond saturation.[16–20] High-precision heavy-ion experiments on pion and kaon dynamics[17,21] revealed more details of the in-medium hadronic properties.[22–26] A soft nuclear EoS at high baryon densities up to $(2-3)$-times the saturation density was predicted from transport theoretical strangeness production analyses.[22–29]

One realized soon a non-trivial density dependence of the EoS. The rise and fall of collective flow with increasing energy was a hint for sudden changes in the softness of the nuclear EoS at high densities.[30–32] More than one decade passed to obtain more constraints on the EoS of highly compressed matter. The recent astrophysical measurements of neutron stars with masses of $1.97 \pm 0.04\ M_\odot$[33] and $2.01 \pm 0.04\ M_\odot$[34] brought more controversial insights on the high-density EoS (see also

the recent work by Fonseca et al.[35] and the review article be Oertel et al.[36]). These observations provide lower bounds for the maximum neutron star mass, excluding a soft EoS at high baryon densities. Neutron stars exhibit a complex internal structure.[37–41] For instance, strangeness carrying mesons (kaons) and baryons (hyperons) can appear in the neutron star interior. In fact, the presence of hyperons (Λ, Σ, Ξ- and Ω) inside neutron stars is in principle energetically allowed, since their chemical potentials are sufficiently large at high baryon densities. Nuclear matter with hyperons weakens the EoS largely at high baryon densities. Several nuclear models, successfully applied to nuclear systems (finite nuclei, heavy-ion collisions), cannot explain the observed data of neutron star masses, if they include hyperons in their descriptions. This is known as the "hyperon puzzle" issue. A recent and nice review on this controversial topic can be found in Refs. 42, 43.

It is thus important to understand better the strangeness part of the hadronic EoS. This is a difficult task due to the lack on detailed experimental information. In fact, for the nucleon-nucleon (NN) interaction (strangeness content $S = 0$) high precision 4300 scattering data are available. They allow an accurate determination of the in-medium NN-interaction, at least for densities close to saturation. Adding strangeness to the system ($|S| = 1$) the situation changes largely. In the $S = -1$-sector (hyperon-nucleon) one has so far had access to 38 scattering data only. They still allow a reasonable determination of the $S = -1$ hyperon-nucleon (YN) interactions, however, with remaining ambiguities particularly for the in-medium YN-potentials. The higher strangeness domain, $S = -2$, is still an unobserved experimental region. Only theoretical predictions are available in the literature. Finally, the $S = -3$ sector concerning ΩN-interactions has been up to present rarely explored.

The YN-interactions are formulated on a group-theoretical basis, such as SU(3) symmetry. Besides SU(3) often SU(6) symmetry is employed. There exist phenomenological Skyrme-like approaches[44] and covariant models. The latter are based on the Relativistic Mean-Field (RMF) theory, firstly introduced by Dürr[45] and Walecka,[46] considerably improved by Bodmer and Boguta[47] and further developed by Serot and Walecka.[48] This RMF framework has been extended to the description of nuclear matter with hyperons.[49–51] Alternatively one can use RMF with density dependent coupling constants to mimic the microscopic non-linear structure of the interaction. The Density Dependent Hadronic (DDH) approaches[52–54] have been applied to matter with hyperons too.[55,56] The microscopic approaches consider higher order correlations in the spirit of the ladder approximation. They are known in the literature as non-relativistic Brueckner-Hartree-Fock[57,58] or covariant Dirac-Brueckner-Hartree-Fock models.[59] They are based on the One-Boson-Exchange (OBE) picture of the baryon-baryon interaction.[60,61] Further theoretical works toward a description of the full octet and decuplet baryons exist. Prominent examples for the $|S| = 1$ YN-interaction are the models of the Nijmengen,[62–65] Jülich[66–68] and Kyoto-Niigata[69–71] groups. Recently, QCD inspired approaches have

been also developed and lattice QCD simulations have been applied to the YN-interactions.[72–74] Chiral effective field (EFT) theory has been also used for the construction of realistic in-medium YN-potentials.[75–78]

The theoretical models for the YN-interactions, in free space and inside the hadronic medium, provide the essential physical input for transport studies of in-medium reactions induced by heavy-ions or hadrons impinging on nuclear targets. In relativistic collisions between heavy-ions or hadrons and nuclei one can probe the in-medium dynamics of produced hyperons and hyperfragments. Thus, such reaction studies can give useful information on the in-medium YN interaction by a systematic comparison with experimental data of produced hyperons and bound hypernuclei. Hypermatter is here of particular importance. While in single-Λ hypernucleus the $|S| = 1$ sector of the YN-interaction can be investigated, hypernuclei with higher strangeness content can be used to explore the higher strangeness part of the in-medium hyperonic interactions. Nuclei with more than one bound hyperons are referred to as multi-strangeness hypernuclei or superstrange nuclei. The denotation "superstrange" and the idea of looking at superstrange nuclei goes back to the pioneer work of Kerman and Weiss[79] with first estimations on multi-Λ hyperfragment yields.

Hadronic in-medium collisions are described theoretically by kinetic theory, introduced by Ludwig Boltzmann in the year 1872.[80] Boltzmann formulated a transport equation for classical many-body systems based on Liouville's theorem. Vlasov extended the Boltzmann equation by including a mean-field potential, followed by the famous work of Uehling and Uhlenbeck taking Pauli blocking effects in binary collisions into account.[81] Since then different theoretical aspects of transport dynamics were investigated. Kadanoff and Baym derived the kinetic equations from non-relativistic quantum statistics.[82] Danielewicz introduced another microscopic derivation of the kinetic equations and applied them for the first time to the dynamics of heavy-ion collisions.[83] Bertsch and Das Gupta continued the transport theoretical studies with more details concerning mean-field and collision dynamics.[84] A modern covariant derivation of relativistic kinetic equations was formulated by Botermans and Malfliet,[85] based on the microscopic Dirac-Brueckner-Hartree-Fock formalism. A more pedagogical introduction to relativistic kinetic theory can be found in De Groot.[86] Since then various models based on (relativistic) kinetic theory have been applied in in-medium hadronic reactions. They are known in the literature as Boltzmann- Uehling-Uhlenbeck (BUU),[87] relativistic BUU (RBUU),[88–90] Giessen-BUU (GiBUU),[91] Hadron-String-Dynamics (HSD),[92,93] Quantum-Molecular-Dynamics (QMD),[94–96] relativistic QMD,[97–99] Fermionic-Molecular-Dynamics (FMD)[100] and Antisymmetrized-Molecular-Dynamics (AMD).[101] A hydrodynamical description of heavy-ion collisions is also possible (see for details Ref. 102).

Nowadays transport theory is further developing to explore (among other tasks) in-medium single- and multi-strangeness dynamics.[103–115] These studies have been motivated by a series of ongoing and forthcoming experimental activities, nicely

reviewed in Ref. 116. The Hyperon-Heavy-Ion (HypHI) collaboration[117] has recently reported longitudinal momentum spectra of low-mass single-Λ hypernuclei in intermediate energy collisions between low-mass nuclei.[118] Within the J-PARC experimental project[119] high energy proton beams will be used for the production of bound hypersystems. We emphasize further experimental activities concerning hypernuclear studies, such as STAR (RHIC),[120] ALICE (LHC),[121] FOPI and HADES at CBM[122,123] and NICA.[124] The forthcoming $\overline{\mathrm{P}}$ANDA experiment at FAIR[125] is of great interest concerning multi-strangeness hypernuclear physics. Indeed, in-medium collisions with antiproton-beams at intermediate energies of few GeV only can overcome the high production thresholds of hyperons. The high annihilation cross sections at low incident energies into multiple meson production (antikaons) and the formation of strangeness resonances can accumulate energy and strangeness content via secondary scattering. Thus, a copious production of heavy hyperons through a multi-step collision process is possible.

We review in detail the theoretical description of in-medium production of hypermatter in hadron- and ion-induced reactions. Section 2 deals with the theoretical details of the superstrange transport dynamics including the treatment of fragment and hyperfragment formation. Results of transport theoretical calculations are given in Sections 3 and 4. In Section 3 we discuss the production of hypermatter in heavy-ion collisions, while Section 4 is devoted to the formation of multi-strangeness hypersystems in hadron-induced reactions. Section 5 summarizes this review.

2. Transport theoretical description of hadronic reactions

There are several ways to derive the kinetic equations. One is based on the field-theoretical covariant description of strongly interacting many-body systems.[126,127] It starts from the non-equilibrium Green's functions of a many-body system. The various many-particle Green's functions are connected with each other through Dyson equations. Restricting up to 2-particle correlations, one can derive within the Schwinger-Keldysh formalism relativistic kinetic equations for a correlated Green's function, which is related to a single-particle phase-space density. Further kinetic equations are obtained for spectral Green's functions, ending up with four coupled kinetic equations. The advantage of this derivation is a direct connection to the microscopic Dirac-Brueckner theory[85] and a natural interpretation of the approximations (semi-classical limit and quasi-particles).

Another simpler derivation is based on Quantum Hadrodynamics, which we follow here.[90] The advantage of this method is the direct relation to the more practicable mean-field theory of QHD.[48] The starting point is the QHD Lagrangian density

$$\begin{aligned}\mathcal{L}_{QHD} =& \overline{\Psi}\gamma_\mu \left(i\partial^\mu - g_\omega\omega^\mu - g_\rho\vec{\tau}\,\vec{\rho}^{\,\mu}\right)\Psi - \overline{\Psi}(m - g_\sigma\sigma - g_\delta\vec{\tau}\,\vec{\delta})\Psi \\ &+\mathcal{L}_\sigma + \mathcal{L}_\omega + \mathcal{L}_\delta + \mathcal{L}_\rho\,. \end{aligned} \tag{1}$$

It includes the free Lagrangians for the Dirac spinors, which is explicitly given, and the free Lagrangians of the exchange $\sigma-, \omega-, \rho-$ and $\delta-$mesons. The mesonic degrees of freedom differ from each other in their internal Lorentz structure. The σ-field is a Lorentz-scalar, iso-scalar meson, the ω-field is a Lorentz-vector, iso-scalar meson, the ρ-field is a Lorentz-vector, iso-vector meson, and finally, the δ-field is a Lorentz-scalar, iso-vector meson. These mesons are responsible for the interaction between the spinors in the spirit of the OBE-model.[60,61] In the following derivations the ρ- and δ-contributions will be omitted for simplicity. The meson field operators are replaced with their classical expectation values and constitute the classical mean-field (or Hartree) potential between the quantal spinor fields. From Eq. (1) one obtains the entire information for a physical system in the mean-field approximation. The energy and pressure densities are defined through the conserved energy-momentum tensor, i.e. the EoS. Furthermore, the Euler-Lagrange equations for the different degrees of freedom are derived, the Klein-Gordon and Proca equations of motion for the virtual mesons and the Dirac equation for the spinors. Latter is used for the derivation of the transport equation and reads

$$\gamma_\mu \left(i\partial^\mu - g_\omega \omega^\mu\right) \Psi - (m - g_\sigma \sigma)\Psi = 0\,. \tag{2}$$

The derivation of the transport equation starts from the Wigner function

$$F_{\alpha\beta}(x,k) = \frac{1}{(2\pi)^4} \int d^4R e^{-ik_\mu R^\mu} < \hat{\overline{\Psi}}_\beta(x + \frac{1}{2}R)\hat{\Psi}_\alpha(x - \frac{1}{2}R) > \quad . \tag{3}$$

This is the so-called Wigner-transformation of the correlated Green's function, which will be related with the 1-body phase-space distribution $f(x,k)$. Note the matrix structure of the Wigner function, indicated in Eq. (3) by the greek subscripts in the spinors Ψ and $\overline{\Psi}$. This matrix notation will be omitted in the following.

With the help of the definition of the Wigner function, Eq. (3) and the Dirac equation (2) the following expression can be verified ($x_1 = x + \frac{1}{2}R$; $x_2 = x - \frac{1}{2}R$)

$$\begin{aligned}\Big(\gamma_\mu(\partial^\mu - 2ik^\mu) + 2im\Big)F(x,k) = \tfrac{2}{(2\pi)^4}\textstyle\int d^4R e^{-ik_\mu R^\mu} \\ < \hat{\Psi}(x_1)\Big(\gamma_\nu \partial^\nu_{x_2} + im\Big)\hat{\Psi}(x_2) > \qquad .\end{aligned} \tag{4}$$

The right-hand side of Eq. (4) can be re-written with the help of the Dirac equation as

$$\frac{2i}{(2\pi)^4} \int d^4R e^{-ik_\mu R^\mu} < \hat{\overline{\Psi}}(x_1)\Big(g_\sigma \hat{\sigma}(x_2) - g_\omega \gamma_\mu \hat{\omega}^\mu(x_2)\Big)\hat{\Psi}(x_2) > \quad . \tag{5}$$

In the mean-field approximation the mesonic fields are just $\mathcal{C}$-numbers. Therefore, they can be taken out of the expectation values. Using the identity

$$g(x_2) = g(x - \frac{1}{2}R) = e^{-\frac{1}{2}R_\mu \partial^\mu_x} g(x) \tag{6}$$

the expression Eq. (5) can be transformed into the expression

$$\frac{2i}{(2\pi)^4}\int d^4R e^{-ik_\mu R^\mu}\left[e^{-\frac{1}{2}R_\mu\partial_x^\mu}\left(g_\sigma\sigma(x)-g_\omega\gamma_\mu\omega^\mu(x)\right)\right] < \hat{\overline{\Psi}}(x_1)\hat{\Psi}(x_2) > \quad . \quad (7)$$

Furthermore, using the identity

$$\int d^4R e^{-ik_\mu R^\mu} e^{-\frac{1}{2}R_\mu\partial_x^\mu} = e^{-i\frac{1}{2}\partial_\mu^k\partial_x^\mu}\int d^4R e^{-ik_\mu R^\mu} \quad (8)$$

the right-hand side of Eq. (4) can be written as

$$2ie^{-\frac{1}{2}\partial_\mu^k\partial_x^\mu}\Big(g_\sigma\sigma(x)-g_\omega\gamma_\mu\omega^\mu(x)\Big)F(x,k) \quad . \quad (9)$$

Thus, for the Wigner function $F(x,k)$ the following equation of motion is obtained

$$\Big(\gamma_\mu(\hbar\partial^\mu-2ik^\mu)+2im\Big)F(x,k) = 2ie^{-\frac{1}{2}i\hbar\Delta}\Big(g_\sigma\sigma(x)-g_\omega\gamma_\mu\omega^\mu(x)\Big)F(x,k)\,, \quad (10)$$

with the triangle-operator Δ defined by $\Delta\equiv\partial_\mu^k\partial_x^\mu$.

The $\hbar$-constant has been explicitly included in Eq. (10) to understand better the semi-classical prescription. This approximation is manifested in a Taylor expansion of the exponential function in Eq. (10) up to first order in $\hbar$, which requires smooth behavior of fields and Wigner function in phase space. This approach is semi-classical in the sense, that the mean-field dynamics is treated classically, while quantal effects are included in the collision integral via Pauli blocking factors. The classical treatment is justified for reaction energies close to the Fermi energy and above, where the de Broglie wave length is small compared to the considered scales of few fm.

A Taylor expansion up to first order of Eq. (10) leads to the following expressions

$$[\gamma_\mu k^{*\mu}-m^*]F(x,k)=0 \quad (11)$$

and

$$\Big(\gamma_\mu\partial^\mu-\Delta(\Sigma_s(x)-\gamma_\mu\Sigma^\mu(x))\Big)F(x,k)=0 \quad (12)$$

for the imaginary and real parts of Eq. (10), respectively. Here in-medium self-energies were introduced, which contain the mean-field potential. The Lorentz-vector (Σ^μ) and the Lorentz-scalar (Σ_s) parts define effective masses and kinetic momenta according

$$k^{*\mu} = k^\mu - g_\omega\omega^\mu = k^\mu-\Sigma^\mu \quad (13)$$

$$m^* = M - g_\sigma\sigma = M-\Sigma_s\,. \quad (14)$$

The imaginary part, Eq. (11), includes already the quasi-particle approximation. That is, the in-medium on-shell constraint for quasiparticles, which are characterized by an effective mass m^* and a kinetic momentum $k^{*\mu}$. The real part, Eq. (12), is used to derive the transport equation (without collisions) for the phase-space distribution function. The expression (12) is still a matrix equation in spinor space.

With a decomposition of the Wigner matrix $F_{\alpha\beta}$ into the elements of the Clifford-Algebra

$$F(x,k) = \mathcal{F}(x,k)\cdot\mathbb{1} + \mathcal{V}_\mu(x,k)\gamma^\mu + \mathcal{P}(x,k)\gamma_5 + \mathcal{A}(x,k)\gamma_\mu\gamma_5 + \mathcal{T}^{\mu\nu}(x,k)\sigma^{\mu\nu} \tag{15}$$

we obtain the desired transport equation for the scalar part $\mathcal{F}(x,k)$, which can be identified with the 1-body phase-space distribution function $f(x,k^*)$

$$\left(k^*_\mu\partial^\mu_x + (k^*_\nu F^{\mu\nu} + m^*(\partial^\mu m^*))\partial^{k^*}_\mu\right) f(x,k^*) = 0 \quad . \tag{16}$$

Eq. (16) is known in the literature as the Vlasov equation. That is, the transport equation without the inclusion of binary collisions. $F^{\mu\nu}$ is the field-strength tensor $F^{\mu\nu} = \partial^\mu\Sigma^\nu - \partial^\nu\Sigma^\mu$ and $f(x,k^*)$ the phase-space distribution function.

The Vlasov equation (16) describes the dynamics of the phase-space under the influence of a mean-field in terms of in-medium scalar and vector self-energies. This phase-space distribution fulfils Liouville's theorem (τ is the eigentime)

$$\frac{d}{d\tau}f(x(\tau),k^*(\tau)) = \left(\frac{\partial x^\mu}{\partial\tau}\partial^x_\mu + \frac{\partial k^{*\mu}}{\partial\tau}\partial^{k^*}_\mu\right) f(x(\tau),k^*(\tau)) = 0 \tag{17}$$

for the invariance of the phase-space distribution. This theorem does not hold any more if collisions are taken into account. In binary processes particles can scatter out of a phase-space volume element (loss term) or into it (gain term). Both terms contribute to the collision integral, which can be derived in a consistent way using the Green's function formalism.[85] Another way of derivation is based on the molecular chaos *Ansatz*.[86] It assumes local collisions in space. The number of binary collisions is proportional to the corresponding 1-particle phase-space distributions. The Pauli principle is taken into account. Combining these assumptions with the Vlasov equation we arrive at the relativistic transport equation. It is known in the literature as the Relativistic Boltzmann-Uehling-Uhlenbeck (RBUU) equation and reads

$$\begin{aligned}
&\left(k^*_\mu\partial^\mu_x + (k^*_\nu F^{\mu\nu} + m^*(\partial^\mu m^*))\partial^{k^*}_\mu\right) f(x,k^*) \\
&= \frac{1}{2}\int \frac{d^3k^*_2}{E^*_2(2\pi)^3}\frac{d^3k^*_3}{E^*_3(2\pi)^3}\frac{d^3k^*_4}{E^*_4(2\pi)^3}\, W(k^*\,k^*_2|k^*_3\,k^*_4) \\
&\times \Big[\, f(x,k^*_3)f(x,k^*_4)\,(1-f(x,k^*))\,(1-f(x,k^*_2)) \\
&\quad - f(x,k^*)f(x,k^*_2)\,(1-f(x,k^*_3))\,(1-f(x,k^*_4))\,\Big],
\end{aligned} \tag{18}$$

with $E^*_j = \sqrt{m^{*\,2} + k^{*\,2}_j}$ for $j = 2,3,4$. The right-hand side gives the temporal changes of the phase-space distribution $f(x,k^*)$ due to binary collisions with other particles, if the Pauli principle allows it. The physical quantity for a scattering process is given by the transition probability $W(k^*\,k^*_2|k^*_3\,k^*_4)$, which is proportional

to the scattering cross section and to a δ-function. Latter ensures energy-momentum conservation for each binary process. Here the formulation was given in terms of kinetic momenta. This is done only for technical reasons and simplifies the numerical calculations considerably.[88] One can use also the phase-space distributions in terms of kanonical momenta. Latter choice is preferable, if the mean-field is explicitly momentum dependent.[91,128]

Numerically the RBUU equation is solved within the test-particle formalism,[129] where the continuous phase-space is discretized by so-called test-particles. Any form of these test particles is allowed. Point-like ones lead, however, to numerical fluctuations in the calculation of densities and, thus, of the mean-field potential. It is more convenient to use a Gaussian form, as proposed by various authors.[88,130] The computational procedure is considerably simplified by the fact of Liouville's theorem. From Eqs. (16) and (17) one obtains the equations of motion for a test particle i ($k = 1, 2, 3$ are the spatial coordinates)

$$\frac{d}{dt}x_i^k = \frac{u_i^k}{u_{i0}} \tag{19}$$

$$\frac{d}{dt}u_i^\mu = \frac{1}{m_i^* u_{i0}}\left(u_{i\nu}F^{\mu\nu} + \partial^\mu m_i^* - (\partial^\nu m_i^*)u_{i\nu}u_i^\mu\right), \tag{20}$$

with the 4-velocity of particle with label i given by $u_i^\mu = (\, u_{i0}, \vec{u}_i\,)$. It is related to the kinetic momentum via the relation $k^{*\mu} = m^* u^\mu$ and fulfils the in-medium on-shell condition $k^{*\mu}k^*_\mu = m^{*\,2}$ or equivalently $u^\mu u_\mu = 1$.

At each time step one calculates the densities and mean-field potentials for each test-particle needed for the solution of the equations of motion (20). Then the collision integral (the right-hand side of the RBUU equation) is numerically treated by a Monte Carlo method. The exclusive elastic and inelastic cross sections are used to determine the final channels. This final state can consist not only of 2 particles, but it can be a multi-particle final state (see below). Then the modulus of the final state momenta is extracted from energy and momentum conservation, and their direction is determined from the differential cross sections. The whole procedure takes place in the local center of mass frame of the two colliding partners. The original method is explained in detail in Ref. 91.

Depending on the reaction type and the beam energy, several exclusive channels must be taken into account in the numerical treatment of the collision integral. For the simulation of heavy-ion collisions and proton-induced reactions up to incident energies of $1-2$ GeV the inelastic channels up to the $\Delta(1232)$ resonance including secondary scattering with pion production and absorption are sufficient. The formation of strangeness at these intermediate energies is a rare process. However, it should be included if one intends to study strangeness production. A more precise treatment of the collision term is possible by considering all baryonic resonances up to 2 GeV, which are given by the Particle Data Group.[131] This is realized in recent developments of transport, such as the UrQMD,[99] HSD[92] and the Giessen-BUU (GiBUU).[91] Latter realization we mostly used for the results of this article.

More details on the cross sections of exclusive primary channels can be found in Ref. 91. With increasing number of primary scattering processes, the number of secondary scattering increases too. Re-scattering is a very important mechanism for the formation of hypernuclei, as we will see later on.

For the mean-field of nucleons different parametrizations exist in the literature. Within a non-relativistic transport equation Skyrme-type interactions are employed.[44] Using the RBUU equation a covariant formulation of the nucleonic mean-field is obviously required. This is achieved by the various parametrizations in the mean-field theory of QHD, which exist in the literature too, see for instance.[91] Essential here are those models with a rather soft EoS, which can describe the collective flow dynamics and kaon production fairly well.[90,91] The mean-field of produced hyperons is constructed from the nucleonic one by SU(3) or SU(6) symmetry arguments.

The mean-field for antiparticles within RMF should be treated with care. As discussed in Ref.132 within a Non-Linear Derivative model,[133] the mean-field approach does not reproduce well the empirical energy dependence of the in-medium proton optical potential, particularly, at high energies. This issue becomes serious in the antiproton case. Indeed, standard RMF models fail to reproduce the empirically known regions of the in-medium $\bar{p}$-optical potential and diverge to infinity with increasing energy. Only a phenomenological re-scaling of coupling constants improves the situation.[134,135] As a standard procedure, transport models use re-scaled couplings for the antiparticle coupling constants.

The transport equation gives the full information on single-particle dynamics of nucleons and produced particles. From the knowledge of the phase-space distribution one can determine thermodynamical properties such as particle densities, energy densities, pressure and the temperature respectively the excitation energy at each phase-space point of the dynamical evolution. This is very useful to gain information on (local) equilibration and the onset of instabilities. The degree of equilibration can be obtained by comparing the transverse and longitudinal components of the local energy-momentum tensor, called transverse and longitudinal pressure. The onset of an instability can be determined by calculating the pressure versus the density at a specific space-point as function of time. Fig. 1 shows the dynamics of thermodynamical quantities, extracted from RBUU calculations. They were obtained at the center of a heavy-ion reaction as function of time. The typical compression/expansion stages appear at intermediate times, as it can be seen from the time dependence of the central density and temperature. Both pressure components (longitudinal and transversal) differ from each other. That is, the participant system is out of local equilibrium. Freeze-out sets in when the particles do not collide any more. Just before freeze-out appears, the pressures are isotropic and local equilibrium occurs. In fact, as shown in Ref. 136, spinodal instabilities appear at the center of participant and spectators at time stages close to freeze-out for heavy-ion collisions at intermediate incident energies. Thus, transport calculations can provide the onset of the fragmentation process, as the consequence of pres-

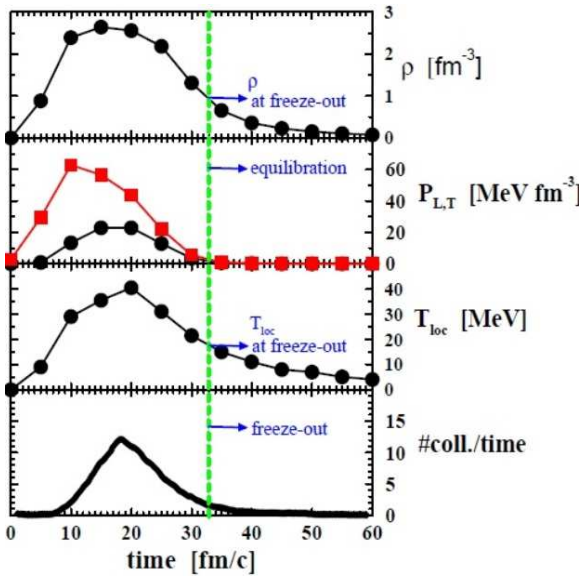

Fig. 1. Time Evolution of the density, longitudinal and transverse pressures (red and black curves in the second graph, respectively), temperature and number of collisions (from top to the bottom) at the central shell of a Au+Au heavy-ion collision at 0.6 GeVbeam energy per nucleon. The vertical line marks the onset of freeze-out.

sure instabilities. Physically this is explained as follows. The matter at densities below saturation intends to reach again the ground state, which is possible only by clusterization and formation of bound fragments.

The fragmentation process can not be described by transport. The propagation of the physical fluctuations is missing, except the stochastic ones in the collision integral. There are attempts to go beyond the single-particle dynamics, see for instance Refs.[101, 137, 138] Furthermore, the mean-field approach for the nuclear potential does not include clusterization processes for dilute matter. There exist recent developments towards this direction. Typel re-formulated the mean-field theory by considering in-medium clusters explicitly in the theoretical framework.[139] In any case, with the knowledge of instabilities and equilibration from transport one can determine when fragmentation sets in and use, as an effective method, more sophisticated statistical models for the clusterization process.

The Statistical Multi-fragmentation Model (SMM)[140, 141] is a well-established approach to describe statistical de-excitation of residual systems. It includes the relevant mechanisms of fragment formation, i.e. evaporation, fission and multi-fragmentation as well as de-excitation of primary fragments. It has been used in hybrid simulations of in-medium hadronic reactions successfully, see for instance Refs. 142, 143, 144. The connection between pre-equilibrium transport and statistical fragmentation models should be done with care. A critical quantity here is the

excitation energy, which is obtained from the transport description of an excited source of hadronic matter, such as spectators in heavy-ion collisions or the residual nucleus in hadron-induced reactions. The excitation energy takes usually values of few MeV per nucleon only. That is, it is comparable with the binding energy per nucleon or even below it. On the other hand, the statistical models are strongly dependent on this quantity,[140,141] most likely due to the non-linear dependence on level densities. Thus, a very accurate determination of the excitation energy is required in transport studies for a reliable application of statistical fragmentation models. This task is closely related with a precise treatment of the initial stage in transport studies. The nuclei used for simulations should be initialized as precise as possible to avoid numerical noise in the temporal evolution of the binding energy and artificial particle emission. The binding energy enters into the calculation of the excitation of the residual source. The particle emission due to numerical fluctuations can affect the extracted mass and charge numbers of the source.

This topic of an accurate initialization has been discussed in detail in Ref.[145] Usually, empirical density profiles of ground state nuclei are used for the construction of initial configurations. This approach can be used for transport simulations at high energies, however, for the purpose of fragmentation with statistical models a better initialization procedure was developed. The density profiles are extracted from relativistic Thomas-Fermi (RTF)calculations by applying the same mean-field model as that used for the propagation of the initial configuration. Furthermore, the inclusion of surface effects in the binding energy and during the propagation is important to achieve a very good stability. As an example, we show in Fig. 2 the temporal evolution of the binding energy and root mean square (rms) radius of a single nucleus, as the result of a transport calculation using 1000 test particles. The filled circle at $t = 0$ fm is the RTF value. As one can see, the improved initialization prescription leads to an almost constant behavior of the binding energy, which is very close to the exact RTF value. Also the rms radius is stable in time, in contrast to the transport calculations with the conventional initialization method. A more detailed picture is given in Fig. 3 in terms of the density profiles. There the proton and neutron density distributions as function of the radial distance are shown. They have been extracted from Vlasov calculations at different times during the simulation of a single nucleus. The RTF reference densities of protons and neutrons are shown too. It is seen that the nucleus is very stable up to long time scales. Only at the surface the Vlasov densities are slightly wider relative to the RTF profile. This is due to the finite width of the Gaussian-shaped test particles. A more detailed discussion on this issue can be found in Ref.[145]

In the following sections we present and discuss the basic features of hypernuclei produced in collisions induced by heavy-ions and in antiproton-induced reactions. We have used the GiBUU model for these simulations. Other transport theoretical studies exist too. They will be discussed aiming to present the recent activities in this field of research.

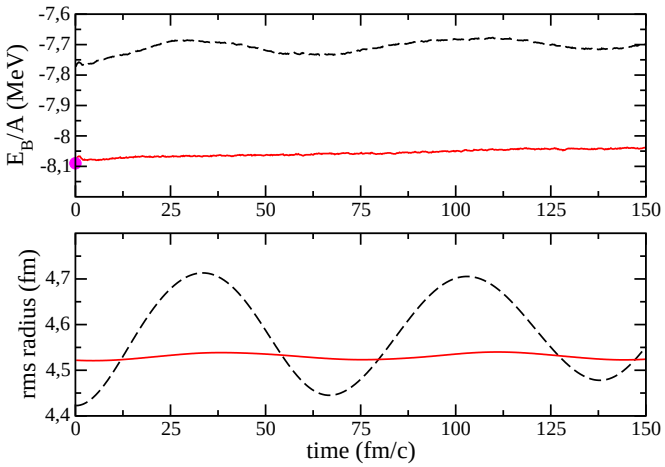

Fig. 2. Binding energy per nucleon (panel on the top) and rms radius (panel on the bottom) as function of time for a ^{112}Sn nucleus. The solid (dashed) curves are obtained from Vlasov calculations using the improved (standard) initialization method. The filled circle symbol at $t = 0$ fm marks the RTF value for the binding energy per nucleon.

3. Strangeness dynamics in heavy-ion collisions

3.1. *General features of reaction dynamics*

We first discuss the general method how pre-equilibrium transport and statistical approaches can be combined into a hybrid model. Proton-induced reactions are very well suited to test such hybrid models. At first, the target remains close to its ground state with moderate excitation. Furthermore, collective effects do not occur, in contrast to the violent compression and expansion dynamics in heavy-ion collisions. According to the transport calculations, in a proton-nucleus reaction the nucleus gets excited by the proton beam. The nucleus starts to emit nucleons (pre-equilibrium emission) and a compound system is formed. As a residual source we define the compound system, which consists of all particles inside the nuclear radius by excluding the emitted nucleons. There are several methods to determine a residual source in transport simulations. One can use either the binding energy of the particles as criterion or apply a density constraint at each particle's position. Assuming that all nucleons inside the nuclear radius belong to the compound system, we define a residual (or fragmenting) source by the density constraint of $\rho_{cut} = 0.01 \times \rho_{sat}$. The particles with a density greater than ρ_{cut} belong to the residual source. Fig. 4 shows the time evolution of the characteristic properties of the residual source. The high energy proton hits the target nucleus. During the beam penetration the target particles are excited due to subsequent collisions. At

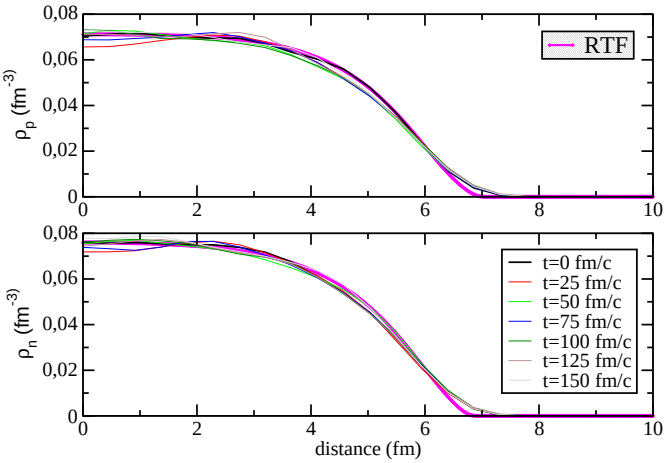

Fig. 3. Density profiles of protons (panel on the top) and neutrons (panel on the bottom) for a ^{112}Sn nucleus. The thick curve in both graphs indicates the RTF density distribution, while the other curves show the same quantity in the Vlasov calculations at different time steps, as displayed.

a time of $t_{fr} \simeq 60 - 70$ fm the residual target is de-excited due to pre-equilibrium particle emission, and the system approaches a freeze-out configuration. The residual system is still slightly excited, since its energy per nucleon (less the nucleon rest mass) is comparable with the ground-state binding energy per particle, but not the same. The difference between them gives the excitation of the system. Depending on the centrality of the proton beam, the value of the excitation energy takes values around 1 MeV and below. The more peripheral the reaction, the smaller the excitation of the residual system.

We estimate the onset of the SMM model at the freeze-out time, i.e. at the time when a stable configuration has been reached. This is indicated in Fig. 4 by the vertical lines. Performing exclusive reactions for all the impact parameter range from central up to most peripheral collisions and applying at each simulation event the SMM model, one arrives to the results of Figs. 5 and 6. There the charge distribution of fragments and differential energy spectra of free neutrons are shown. In particular, the charge distribution reproduces the experimental data fairly well. The evaporation peak close to the initial target charge number $Z_{init} = 79$ and the wide fission peak at around $Z = 79/2$ are clearly visible. These calculations predict also a multi-fragmentation region at low Z-values. This part of the distribution originates mostly from central events. For the formation of hypernuclei not only the mass and charge multiplicities, but also momentum distributions are crucial.

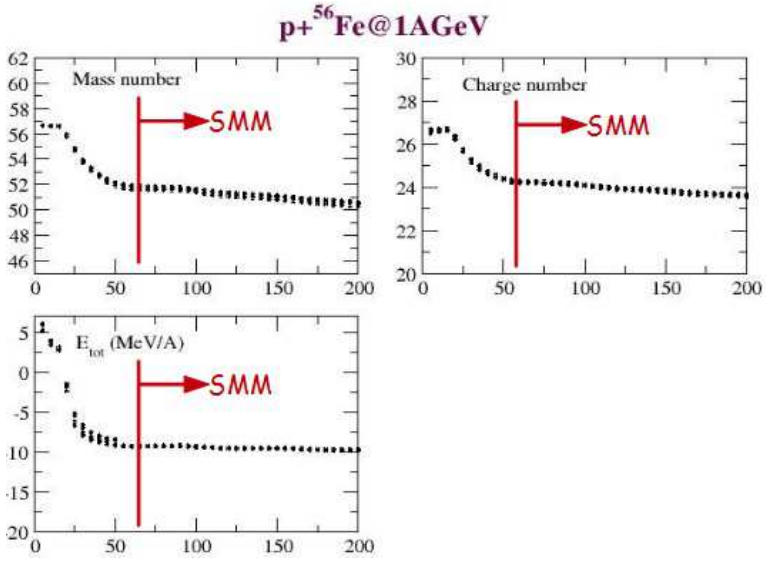

Fig. 4. Mass number, charge number and total energy per nucleon (less the nucleon rest mass) in the panels on the top-left, top-right and bottom-left, respectively, as function of time for the residual target nucleus. The vertical marks in each graph indicate the onset of the SMM model.

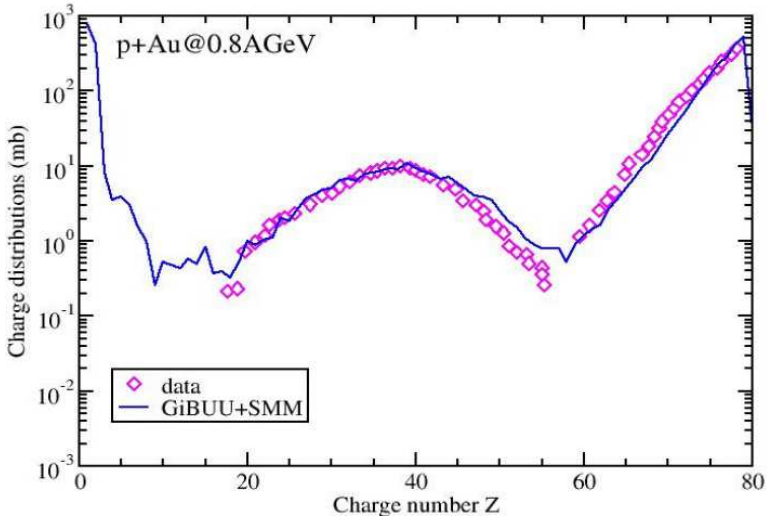

Fig. 5. Charge distribution for the reaction as indicated. Hybrid calculations (solid curve) are compared with experimental data (open symbols) taken from[148,149] (figure taken from[150]).

The comparison of the hybrid calculations with data on differential energy spectra is shown in Fig. 6, for a similar reaction system as in Fig. 5. These spectra are

selected at various polar angles and for free neutrons only. In this figure one realizes the importance of having both, pre-equilibrium and statistical emission. The high energy part of the spectrum with the clear visible quasi-elastic peaks at forward angles results from the particle emission of the transport calculations. The low energy spectrum of emitted particles is then the result of the SMM model due to de-excitation. The combination of both models, GiBUU and SMM, is required to explain the energy spectrum over the entire range.

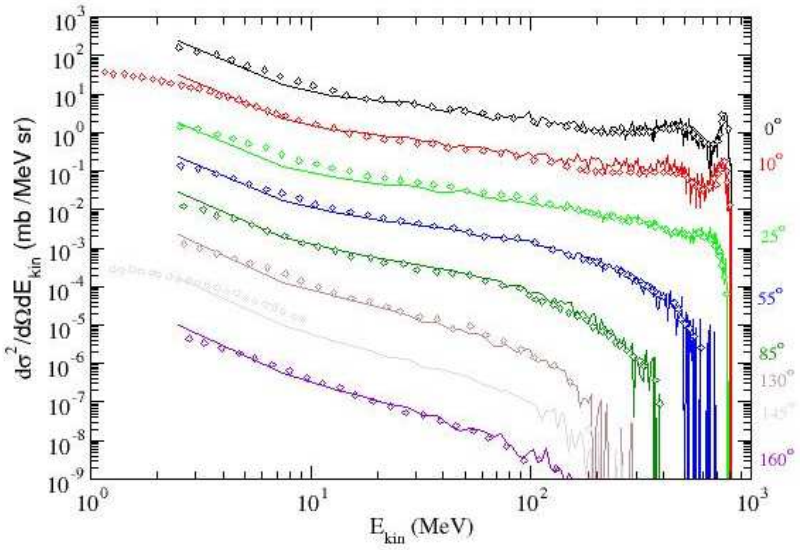

Fig. 6. Kinetic energy spectra of emitted neutrons at different polar angles (as indicated on the right) for p+Pb reactions at 0.8 GeV beam energy. Hybrid calculations (solid curves) are compared with experimental data (open symbols) taken from.[151]

The application of the combined approach in the dynamics of heavy-ion collisions follows in principle the same scheme. The difference with the case of proton-induced reactions are the collective effects. The participant region, which is formed during the pre-equilibrium stage, exhibits a violent compression/expansion dynamics showing up in a strong radial flow component.[146,147] Spectator dynamics, on the other hand, exhibits better controlled conditions. This is shown in Fig. 7, where several properties of spectator matter are displayed as function of time. These are the mass number, the excitation energy, the density and the pressure (at the center of the projectile spectator). The three curves at each panel differ in the centrality. A similar situation appears as in the case of the residual nucleus in proton-induced reactions. After spectator's formation the system is firstly excited before cooling sets in. This can be seen in the graphs of Fig. 7, where the mass number drops to a constant value. However, the system remains after cooling in an excited configuration.

The degree of excitation is relatively high for semi-central collisions (black curves), while with increasing centrality (red and green curves) the excitation decreases. This is due to the less mixing between spectator and highly excited participant matter with rising impact parameter. Note that after ca. 50 fm/c the pressure becomes negative. This means the presence of fluctuations and the begin of the fragmentation process.

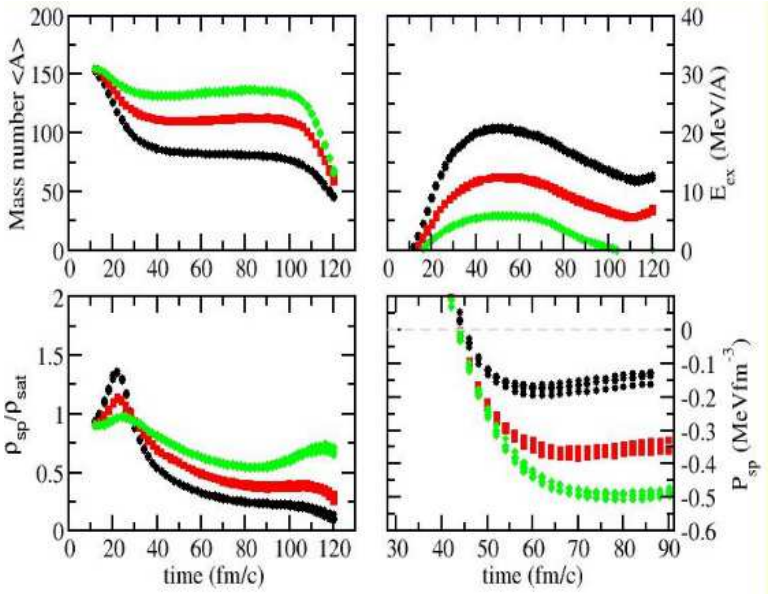

Fig. 7. Time evolution of the mass number (top-left), excitation energy per nucleon (top-right), central density relative to saturation (bottom-left) and central pressure (bottom-right) for projectile spectator in Au+Au collisions at 0.6 GeV beam energy per particle. The centrality increases from black to red and green for each panel.

The question appears at which time step the SMM model should be applied. Here we refer to Fig. 8, where the degree of equilibration is shown. In this figure the ratio between the longitudinal and transverse components of the central pressure in spectator matter is displayed as function of time. It is seen, that after roughly 50 fm/c the ratio approaches unity indicating the onset of local equilibration inside spectator matter. We have well defined conditions in spectator matter. That is, instabilities and equilibration occur at almost the same freeze-out time with a density of around $\rho_{sat}/3$ and a central temperature of $T \simeq 5$ MeV.[136]

Having the mass, charge numbers and the excitation energy of the spectator at freeze-out, one can apply the SMM model for spectator fragmentation. An example of this procedure is shown in Fig. 9. There the velocity distributions of various spectator fragments for a Xe+Pb heavy-ion collision at 1 GeV beam energy per particle

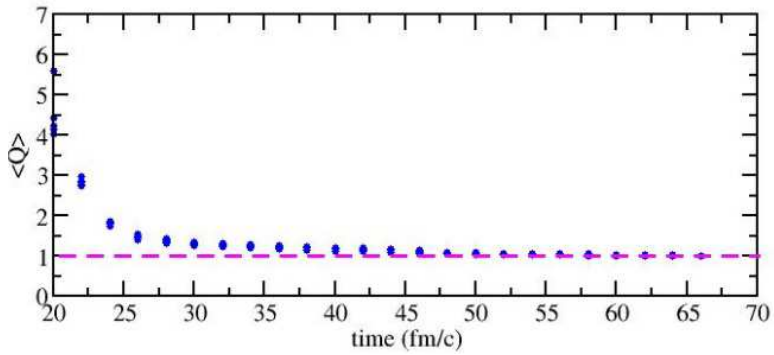

Fig. 8. Ratio between the two pressure components, longitudinal and transversal, for spectator matter for a semi-central Au+Au reaction at 0.6 GeV incident energy per nucleon.

are shown. As one can see, the theoretical calculations reproduce the experimental data[152] satisfactorily. More detailed comparisons including fragment multiplicities can be found in Ref. 103. There exist also other recent studies on spectator fragmentation. In Refs. 142, 143 and 144 the SMM model has been applied to the fragmentation of projectile-like residues in intermediate energy collisions between Sn-isotopes. It is shown that the SMM approach reproduces the experimental isotope distributions fairly well.

3.2. *Dynamics of strangeness and hypernuclei in heavy-ion collisions*

Two features should be described as precise as a model allows for a reliable production of hypermatter. That is, fragmentation and strangeness dynamics. Concerning fragmentation we have shown that this task can be well described by a combination of non-equilibrium transport and statistical approaches. Strangeness dynamics in heavy-ion collisions is consistently described with respect to data on kaons and hyperons[91] (and references therein). We continue the discussion with the production of hypernuclei. Fig. 10 shows the rapidity spectra of produced fragments in projectile and target spectators as well as of hyperons. The fragment distributions are the result of the hybrid simulations, while the hyperons result from the transport calculations only. This figure shows the idea of coalescence for hypermatter production. In fact, a part of the hyperon spectrum overlaps with the fragment longitudinal momentum distributions close to projectile and target rapidities. The Λ-particles are mainly created in primary $BB \to BYK$-collisions and in secondary $\pi B \to YK$-scattering. Elastic and quasi-elastic scattering, i.e., with strangeness exchange, are included too. Secondary scattering involving fast pions is here important to create such a wide spectrum in beam momentum. Thus, some of the produced hyperons with a velocity close to that of spectators can be captured and form hyperfragments. This is realized by a coalescence in coordinate and momentum space between the

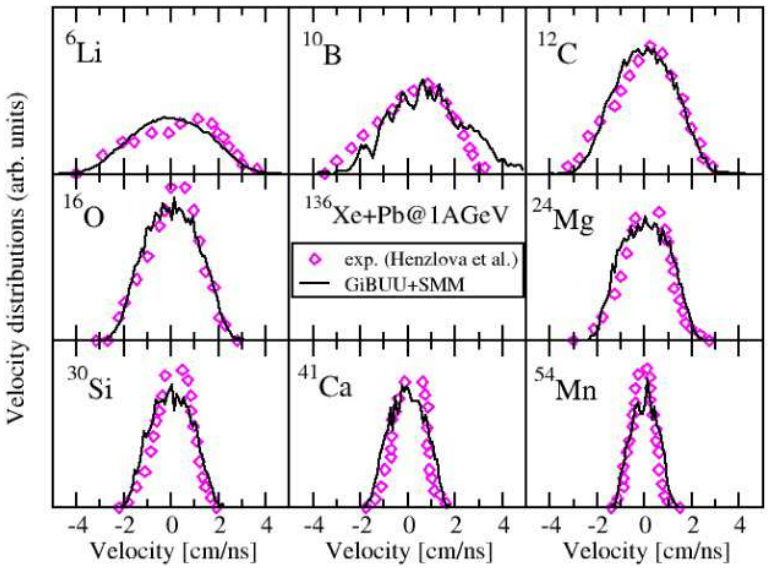

Fig. 9. Velocity distributions for various fragments at the rest-frame of projectile spectator, as indicated. The hybrid calculations (solid curves) are compared with experimental data (open symbols), taken from Ref.[152] (figure taken from[103]).

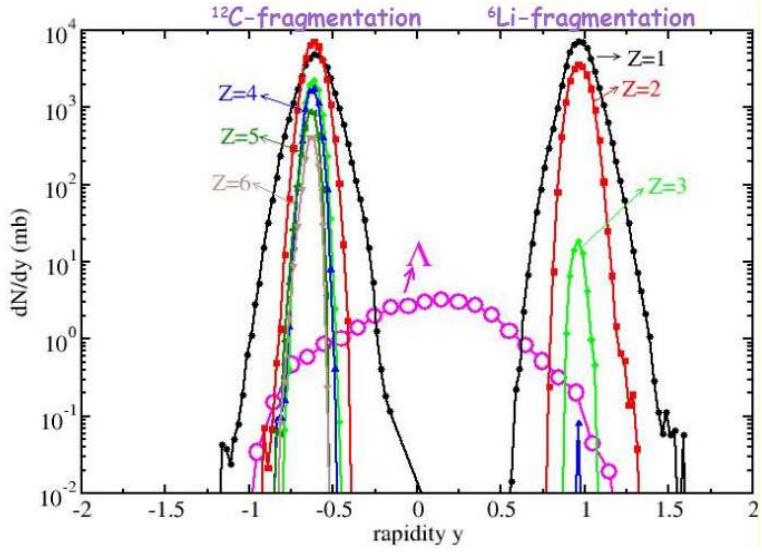

Fig. 10. Rapidity distributions of projectile and target fragments as well as of Λ-hyperons, as indicated, for Li+C heavy-ion collisions at 2 GeV incident energy per nucleon.

hyperons and cold SMM fragments.

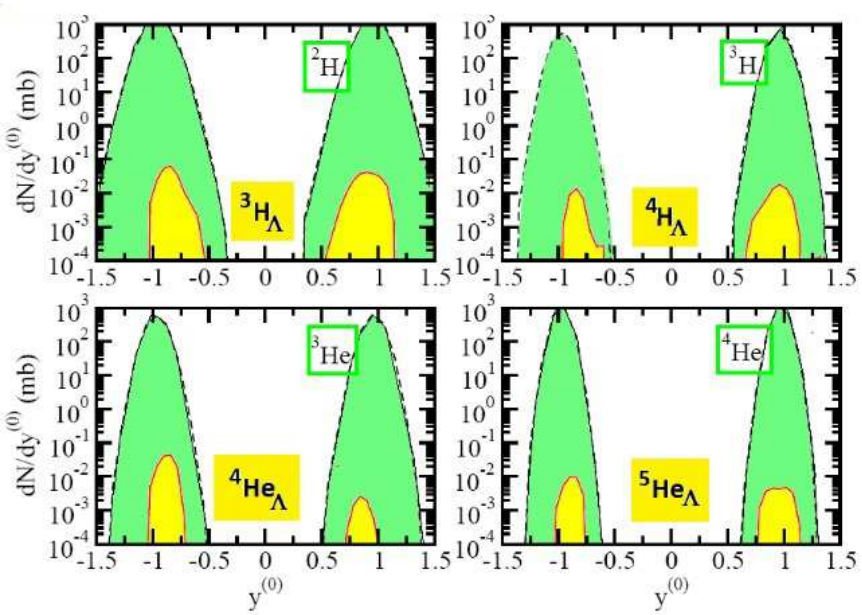

Fig. 11. Rapidity spectra of produced spectator fragments (dashed curves with green area) and the corresponding hyperfragments (solid curves with yellow area), as indicated. The considered reactions are a C+C collisions at 2 GeV incident energy per nucleon.

A typical result of hypermatter formation is shown in Fig. 11. There the rapidity spectra of light-mass spectator fragments with the corresponding hyperfragments are displayed. The considered C+C reaction at 2 GeV beam energy per nucleon has been chosen, since for a similar colliding system (Li-beam on C-target) ongoing experimental activities are in progress.[117,118] On sees in Fig. 11, that the light-mass hypernuclei are produced with relatively low cross sections. Their production rates are in the range of few μb only. The main reason for the low production cross sections is the small size of the colliding systems. The smaller the nucleus, the less secondary scattering. Latter feature is, however, important to de-accelerate the hyperons inside the spectators, so that they can be captured. The predicted values of the light-hypernuclei are very close to the preliminary experimental data.[118] We have used here the symmetric C+C system for the determination of hypernuclei, in order to obtain a better statistics. In any case, it is desired to use colliding systems as heavy as experimentally possible, in order to obtain large hypernuclear cross sections.

At present the study of hypermatter formation in intermediate energy heavy-ion collisions is an active field of research. There exist recent investigations by other groups. They use alternative approaches of transport dynamics combined with po-

tential, coalescence and statistical prescriptions for the description of the fragmentation process. In Ref. 114 the well-established isospin-QMD transport model in combination with a newly developed fragmentation algorithm[115] has been applied in collisions between heavy-ions. They have studied the formation of light-mass hypermatter in heavy-ion reactions at energies just above the kaon production threshold. As an important outcome of their analysis, it was found that rescattering strongly affects the hypernuclear formation. In Refs. 108 and 109 the Dubna-Cascade and the Ultra-relativistic QMD (UrQMD) kinetic approaches have been adopted for the dynamical treatment of heavy-ion collisions, in combination with potential and coalescence prescriptions for the formation of hypermatter. Their studies show the possibility of hypernuclear formation in heavy-ion reactions at intermediate energies. Even the production of multi-strangeness hypersystems is favorable with rather high cross sections, however, using heavy-mass projectile and target nuclei. For instance, single- and double-hypernuclei in spectator fragmentation are produced with cross sections of few mb and μb, respectively, in Pb+Pb collisions around 1 GeV incident energy per particle. Bound hypermatter with $|S| = 3$ is also predicted with cross section in the μb-region at higher beam energies above 2 GeV per nucleon. The authors of Ref. 110 have used the UrQMD and HSD transport models in combination with a coalescence of baryons (CB) for the description of the in-medium hyperonic capture. In particular, they have applied the hybrid UrQMD+CB and HSD+CB approaches to collisions between heavy-ions of different size at projectile energies per particle above 2 GeV per nucleon. In their analysis the formation mechanism of hyperfragments originating not only from residual spectators, but also from the participant region, has been studied in detail.

4. Multi-strangeness dynamics in antiproton-induced reactions

In in-medium $\bar{p}$-reactions strangeness particles are produced in annihilation processes close to the low-density surface region of the nucleus. Depending on the centrality, this perturbation can penetrate deep into the nucleus through multi-step binary processes. The average excitation per nucleon is comparable to that of the proton-nucleus reactions. This is shown in Fig. 12 in terms of the time evolution of average mass, charge and excitation energy per particle for both type of reactions. However, the main difference between p- and $\bar{p}$-induced reactions shows up in the abundance of produced particles, as it can be seen in Fig. 13. Generally, the multiplicity of all produced particles increases in the $\bar{p}$-case. In particular, the multiplicity of antikaons and Λ-hyperons increases largely in the $\bar{p}$-induced reactions and the heavy Ξ-baryon appears. This is due to the strong annihilation cross sections mainly into multi-mesonic final states.[153] Furthermore, the annihilation into hyperon-antihyperon pairs becomes less and decreases by an order of magnitude with increasing mass of the produced (anti)hyperons. On the other hand, secondary scattering involving the cascade particles will be important for the for-

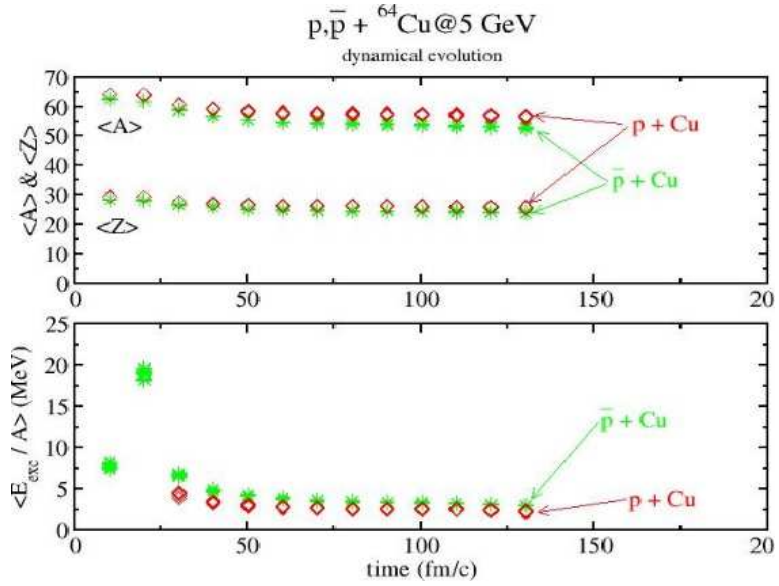

Fig. 12. Time evolution of the average mass number, charge number (upper panel, as indicated) and the average excitation energy per nucleon (lower panel) of the residual nuclei. GiBUU calculations for proton-induced (open diamonds) and antiproton-induced (filled stars) reactions at an incident energy of 5 GeV and impact parameter of b=3.4 fm are shown.

mation of superstrange matter, as we will see. The fragmentation process here (see Fig. 14) is very similar to the p-induced reactions, as it can be seen in Fig. 5. Again, evaporation, fission and multifragmentation regions are visible going from most peripheral to most central reactions.

Fig. 15 summarizes the results of the pre-equilibrium transport and SMM calculations in terms of the rapidity distributions of produced residual fragments and hyperons. The Λ-rapidity spectrum is rather broad. Secondary scattering is responsible for the low energy part of produced Λ-particles. This supports the formation of Λ-hypernuclei, as in the case of spectator fragmentation in heavy-ion collisions. The most interesting part here is the Ξ-production, which will be responsible for the production of multi-strangeness hypermatter. Ξ-particles are created with rather high probability, even if their production cross sections from annihilation are very low. In fact, while $\Lambda\bar{\Lambda}$-pairs are produced with cross sections of several hundred μb, the antiproton annihilation cross section for Ξ-production is very low with orders of few μb only.[154]

Most of the Ξ-hyperons escape the nucleus, but there is a small fraction with rapidities close to those of the residual fragments. Due to the high production threshold of the heavy $\Xi(1315)$-particles one would naively expect that they escape the nucleus with high rapidities. However, secondary scattering of produced Ξ-hyperons with the hadronic environment is crucial for low energy cascade particles.

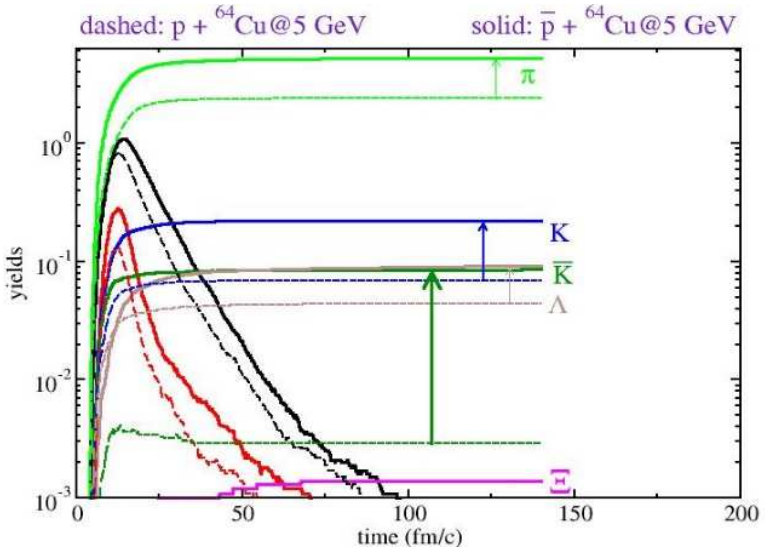

Fig. 13. GiBUU results for the particle yields as function of time for the same reactions as in Fig. 12. The vertical arrows indicate the change of particle yields going from p-induced (dashed curves) to $\bar{p}$-induced reactions (solid curves). The different colored curves denote the various particles, as indicated. The black and red curves, which drop fast in time, correspond to Δ and higher resonances, respectively.

This is manifested in Fig. 16 in terms of momentum spectra of the total Ξ-yield including the exclusive contribution channels. Indeed, secondary scattering processes involving (anti)kaons, and kaonic/hyperonic resonances contribute largely to the low energy tail of the Ξ-momentum distribution. The situation is similar for the momentum spectra of produced Λ and Σ hyperons in $\bar{p}$-induced reactions, where experimental data exist.[155]

The formation of not only single-Λ hypernuclei, but also of double-Λ hypermatter is possible in $\bar{p}$-induced reactions. However, the probabilities of $|S| = 2$-hypermatter are still very low with respect to Λ-hypernuclear yields.[104] An alternative method has been proposed by the $\overline{\mathrm{P}}$ANDA -collaboration to enhance the production of superstrange bound matter.[125] That is a two-step reaction with primary and secondary targets. An antiproton beam interacts with a first target. The low energy part of the produced Ξ-hyperons can be used as a secondary beam for Ξ-induced reactions on the secondary target. The interaction between the Ξ-particles with the particles of the secondary target can create multiple captured hyperons and, thus, multi-strangeness hypernuclei. Indeed, transport-theoretical studies support this scenario.[104]

Fig. 17 shows the strangeness dynamics for Ξ-induced reactions at three different low energies of the Ξ-beam. Two aspects are visible here. At first, a significant capture of Λ-particles inside the matter is observed. Secondly, this feature shows

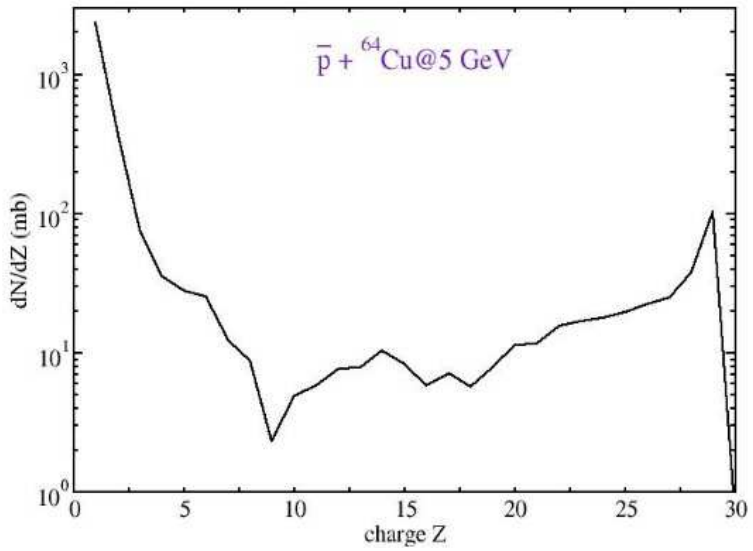

Fig. 14. Fragment charge distribution for centrality-inclusive $\bar{p}$-induced reactions, as indicated. The curve is the result of the GiBUU+SMM hybrid approach.

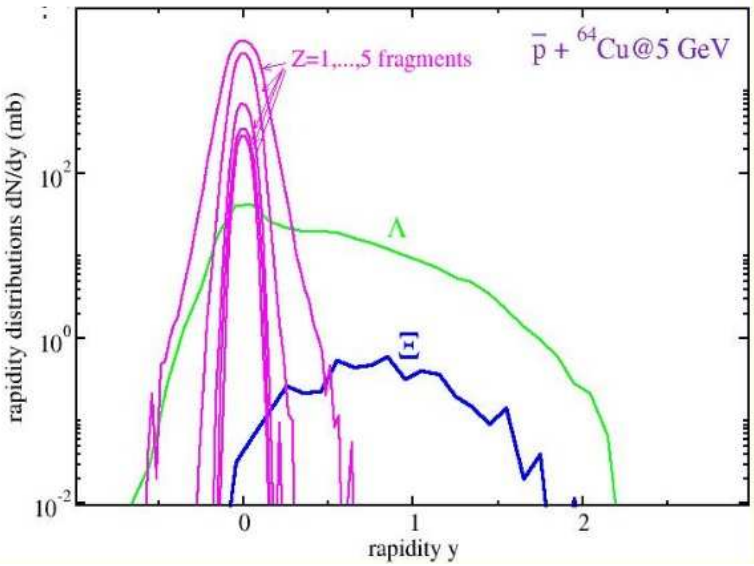

Fig. 15. Rapidity spectra of different fragments, Λ- and Ξ-hyperons for the same reaction as in Fig. 14. The curves result from GiBUU+SMM hybrid calculations (figure taken from[104]).

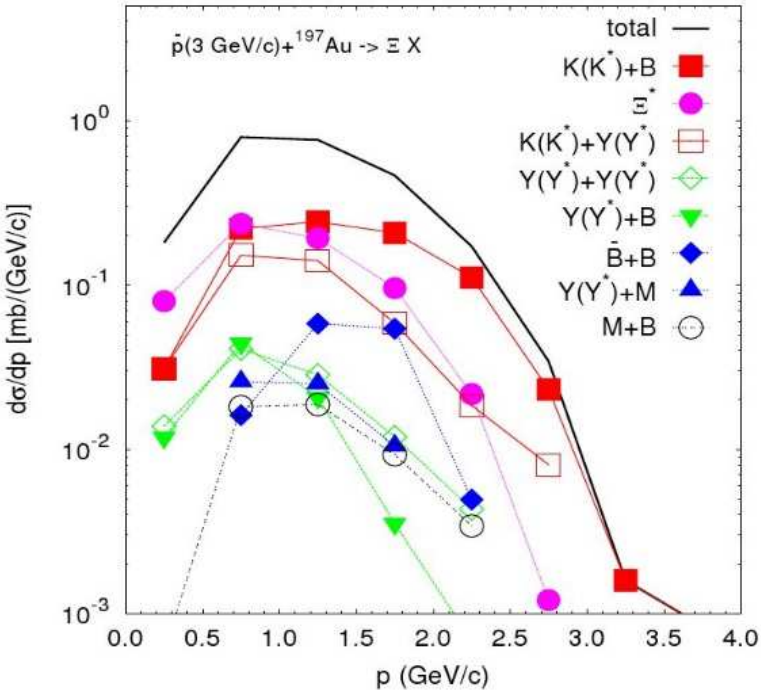

Fig. 16. GiBUU results for the momentum spectrum of inclusive Ξ-production (solid curve) together with the partial contributions to the total Ξ-production for the antiproton-induced reaction, as indicated (figure taken from[153]).

a strong energy dependence. The main mechanism of Λ-production here is the inelastic $\Xi N \to \Lambda\Lambda$ channel. According to microscopic calculations[156,157] this cross section can increase largely at low Ξ-energies with respect to elastic $\Xi N \to \Xi N$-scattering. Thus, double Λ production drops with increasing energy of the cascade particles. This energy dependence in transport calculations is very strong and reflects just the strong energy dependence of the corresponding cross section.[156,157] Note that for these important channels no experimental data exist, in contrast to $|S| = 1$-scattering.[67–71]

Formation of double-strangeness ΛΛ hypernuclei can thus occur in the secondary reaction. This is shown in Fig. 18, where the charge distributions of fragments (upper panel) and ΛΛ-hyperfragments (lower panel) at different Ξ-energies are shown. At first, the fragment distribution becomes broader with increasing beam-energy of the cascade particles. Higher incident energy is associated with increasing excitation of the residual target nucleus. Thus, the fission region at around half the initial target charge and multi-fragmentation show up with rising beam energy. As an important result, an abundant production of $|S| = 2$-hypernuclei is predicted by these transport calculations. This is visible in Fig. 18 by comparing corresponding

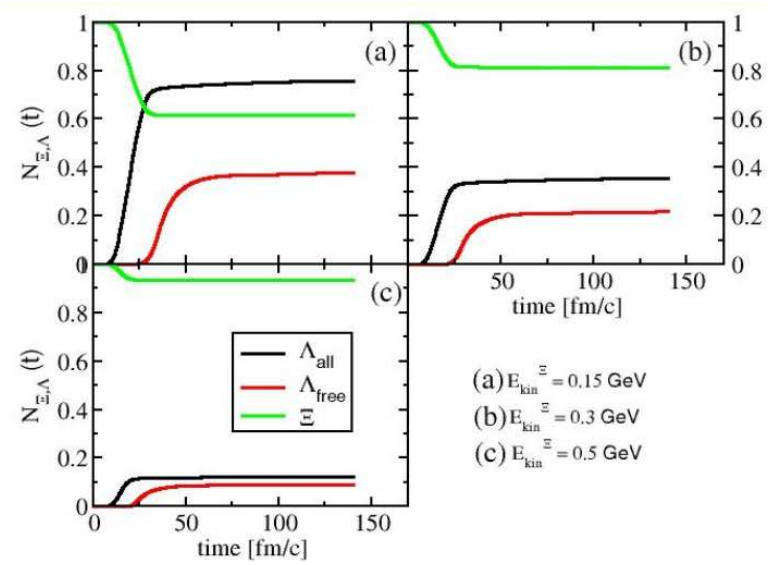

Fig. 17. GiBUU calculations for the total yields (normalized to unity at $t = 0$ fm/c) of Λ (black curve) and Ξ (green curves) particles as function of time for Ξ-induced reaction on Cu-target at three beam energies. The red curve show the yield of free Λ-hyperons only.

curves for fragments (upper panel) and hyperfragments (lower panel) for each incicent Ξ-energy. With increasing beam energy the production of hypermatter around the evaporation peak drops significantly. However, the production yields of double-strangeness $\Lambda\Lambda$-hypernuclei are in the mb-region at these low Ξ-energies.

Therefore, the proposed $\overline{\mathrm{P}}$ANDA -experiment can be very well suited to explore in more detail not only the nucleon-hyperon interactions, but also the still less understood regions of the higher strangeness sectors. Recent theoretical activities have investigated the in-medium hyperon interactions for $|S| > 1$.[62–64, 156, 157] These are based on the microscopic meson-exchange picture or using quark-cluster approaches. The predictions between the theoretical models differ to a large extend. Therefore, a parameter-free theoretical framework would be obviously desired. This is possible only if one goes beyond the meson-exchange picture and considers the internal hadron structure. Recent attempts in this direction have been started within the more sophisticated Lattice QCD-simulations[72–74] and chiral-EFT theories.[75–78] The formation of multi-strangeness bound matter in $\overline{\mathrm{P}}$ANDA -type reactions can be used as a probe to test the microscopic predictions for the superstrange sector of the in-medium hyperon potential. This issue has been studied recently in detail.[105] An example is shown in Fig. 19, where the mass number distributions of all fragments, double-$\Lambda\Lambda$ hyperfragments and, in particular, Ξ-hyperfragments are displayed using two different approaches for the ΞN-scattering. The transport results on the left are based on the extended-soft-core (ESC) approach,[156] while those on

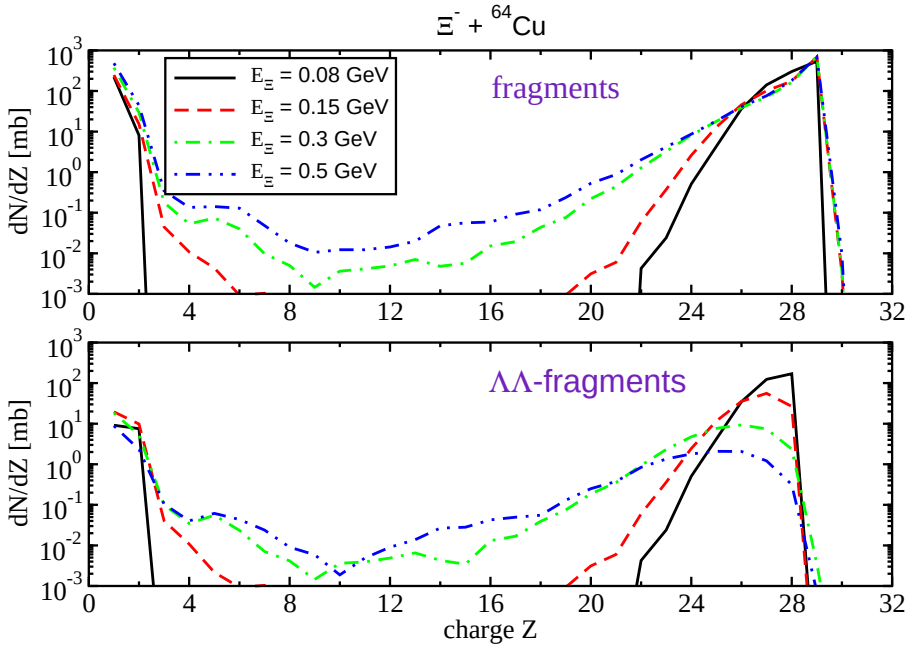

Fig. 18. Charge distributions of fragments (panel on the top) and double-Λ hyperfragments (panel on the bottom) for Ξ-induced reactions at incident energies as indicated (figure taken from[104]).

the right are performed within the quark-cluster model (FSS).[157] Both models lead essentially to different results for ΞN-elastic and inelastic $\Xi N \to \Lambda\Lambda$-scattering. In particular, the FSS $\Xi N \to \Lambda\Lambda$-cross section is strongly reduced relative to the ESC-predictions. Thus, the Ξ-multiplicity increases in the transport calculations using the FSS model. The consequence is a higher production yield of Ξ-hypernuclei, as clearly shown in Fig. 19. Note that the formation of Ξ-hypernuclei beyond the conventional evaporation region is possible depending, however, on the microscopic model applied. The $\overline{\mathrm{P}}$ANDA -proposed scenario could thus be used to better constrain the higher strangeness sector of the in-medium interaction.

5. Summary and conclusions

In summary, in-medium reactions induced by heavy-ions and antiproton-beams represent an excellent tool to study in more detail the multi-strangeness sector of the hadronic equation of state. The knowledge of the in-medium superstrange interactions is crucial not only for nuclear and hadron physics, but also for nuclear

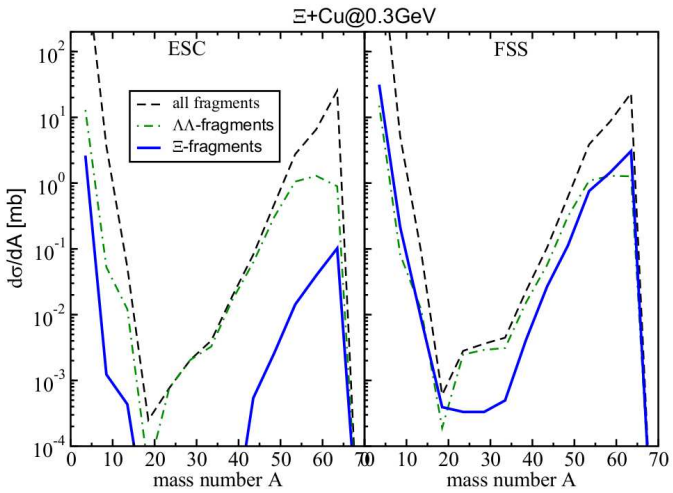

Fig. 19. Mass distributions of fragments (dashed curves), ΛΛ-hyperfragments (dot-dashed curves) and Ξ-hyperfragments (thick solid curves) for Ξ-induced reactions at 0.3 GeV incident energy. Both panels show the results of the GiBUU+SMM model using two different microscopic approaches for the ΞN-interaction (figure taken from[105]).

astrophysics. Furthermore, reaction studies on bound superstrange hypermatter offer great opportunities to explore the unobserved regions of exotic bound hypersystems.

The transport-theoretical description of in-medium hadronic reactions is indispensable for hypernuclear studies. Microscopically developed approaches for in-medium interactions can be probed in complex situations of the reaction dynamics within kinetic approaches. Transport simulations can be also used to simulate the event structure of proposed experiments. A combination of pre-equilibrium dynamics and statistical fragmentation is a very useful tool to understand better the complete dynamics in such reactions, i.e., pre-equilibrium propagation and dynamical particle production as well as statistical fragmentation.

In-medium hadronic reactions offer also other possibilities of study. By extending heavy-ion reactions to heavier colliding systems and to higher beam energies above the strangeness production thresholds, one can probe definitely superstrange matter at baryon densities far beyond saturation. Such a task is theoretically possible and experimentally feasible at the Compressed-Baryonic-Experiment (CBM) at FAIR. Furthermore, hadron-induced reactions, such as proposed by $\overline{\mathrm{P}}$ANDA , but using high energy secondary Ξ-beams can be useful to explore $|S| = 3$-superstrange dynamics involving the heavy Ω(1673)-baryon. The particular nature of the Ω-particle (it consists of three s-quarks) does not allow high production cross sections. In fact,

the Ω-production is a very rare process with cross sections of a few nb only.[154] However, recent transport studies show that secondary scattering increases their production yield in antiproton-nucleus reactions.[106]

In conclusion, the ongoing theoretical activities, presented in this article, are relevant for the forthcoming experiments on in-medium superstrange hypernuclear physics. A more collaborative work between different scientific communities is required to explore in full detail the complex and so far unobserved regions of the nuclear and hadronic equation of state. Hypernuclear physics is a fascinating field of research, which agglutinates the microcosmos of nuclear and hadron physics with the macrocosmos of nuclear astrophysics.

Acknowledgements

The results in this article were obtained in collaboration with many colleagues over the last years. At first, I would like to thank H.H. Wolter, C. Fuchs, Th. von Chossy and M. Weigel from the LMU-Munich, who introduced me into the world of hadron physics. I also would like to thank M. Di Toro, M. Colonna, A. Bonasera, J. Rizzo and G. Ferini for collaborations related to strangeness production. The collaborations with the colleagues from the experimental side were also very important to understand the reliability of the theoretical results. In this respect I would like to thank W. Reisdorf, W. Trautmann, Y. Leifels, N. Hermann, L. Fabbietti, T.R. Saito, C. Rappold and J. Pochodzalla. For intensive discussions I would like to thank the colleagues from other theoretical groups, in particular, A. Botvina, S. Typel, J. Aichelin, C. Hartnack, E. Bratkovskaya, I. Mishustin, P. Danielewicz, A. Ono, and Amand Faessler, among many others. I would like also to thank my greek colleagues, G.A. Lalazissis, Ch. Moustakidis V. Prassa from the Aristotle University of Thessaloniki for further helpful discussions. Finally, a great thank you goes to the Giessen-group. I would like to particularly thank U. Mosel and H. Lenske for their intensive support during my stay in Giessen, and W. Cassing for deep discussions into QCD-related topics. I would like to thank also A. Larionov, N. Tsoneva, and the members of the GiBUU-group, in particular, O. Buss, K. Gallmeister and J. Weil, for many discussions related to theoretical and computational issues. I would like to thank especially M. Kaskulov for the great collaboration concerning the improvement of conventional RMF theory.

References

1. A.M. Poskanzer, *et al.*, *Phys. Rev. Lett.* **35** (1975) 1701.
2. H.H. Heckman, *et al.*, *Phys. Rev. C* **17** (1978) 1651.
3. L.S. Schroeder, *Nucl. Instrum. Methods* **162** (1979) 395.
4. R. Stock, *et al.*, *Phys. Rev. Lett.* **44** (1988) 1243.
5. H. Stroebele, *et al.*, *Phys. Rev. C* **27** (1983) 1349.
6. A. Baden, *et al.*, *Nucl. Instrum. Methods* **203** (1982) 189.
7. A. Gobbi, *et al.* (FOPI Collaboration), *Nucl. Instrum. Methods A* **324** (1993) 156.

8. J. Ritman, *et al.* (FOPI Collaboration), *Nucl. Instrum. Methods (Proc. Suppl.) B* **44** (1995) 708.
9. W. Reisdorf, H. G. Ritter, *Ann. Rev. Nucl. Part. Sci.* **47** (1997) 663.
10. N. Herrmann, J.P. Wessels, T. Wienold, *Ann. Rev. Nucl. Part. Sci.* **49** (1999) 581.
11. P. Danielewicz, G. Odyniec, *Phys. Lett. B* **157** (1985) 146.
12. S. Nagamiya, J. Randrup, T.J.M. Symons, *Ann. Rev. Nucl. Part. Sci.* **34** (1984) 155.
13. K.H. Kampert, *J. Phys. G: Nucl. Phys.* **15** (1989) 691.
14. S. Nagamiya, M. Gyulassy, *Adv. Nucl. Phys.* **13** (1984) 201.
15. H.H. Gutbrod, A.M. Poskanzer, H.G. Ritter, *Rep. Prog. Phys.* **52** (1989) 1267.
16. A. Andronic, *et al.* (FOPI Collaboration), *Phys. Lett. B* **612** (2005) 173.
17. W. Reisdorf, *et al.* (FOPI Collaboration), *Nucl. Phys. A* **781** (2007) 459.
18. A. Andronic, *et al.* (FOPI Collaboration), *Phys. Rev. C* **67** (2003) 034907.
19. J. Lukasik, *et al.* (INDRA and ALADIN Collaborations), *Phys. Lett. B* **608** (2005) 223.
20. A. Andronic, J. Lukasik, W. Reisdorf, W. Trautmann, *Eur. Phys. J. A* **30** (2006) 31.
21. C. T. Sturm, *et al.* [KAOS Collaboration], *Phys. Rev. Lett.* **86** (2001) 39.
22. C. Fuchs, *Prog. Part. Nucl. Phys.* **56** (2006) 1.
23. C. Hartnack, *et al.*, *Phys. Rept.* **510** (2012) 119.
24. W. Cassing, E. L. Bratkovskaya, *Phys. Rept.* **308** (1999) 65.
25. J. Aichelin, C. M. Ko, *Phys. Rev. Lett.* **55** (1985) 2661.
26. A. B. Larionov, U. Mosel, *Phys. Rev. C* **72** (2005) 014901.
27. T. Klähn, *et al.*, *Phys. Rev. C* **74** (2006) 035802.
28. C. Hartnack, H. Oeschler and J. Aichelin, *Phys. Rev. Lett.* **96** (2006) 012302.
29. C. Fuchs, A. Faessler, E. Zabrodin and Y. M. Zheng, *Phys. Rev. Lett.* **86** (2001) 1974.
30. P. K. Sahu, *et al.*, *Nucl. Phys. A* **640** (1998) 493.
31. C. Pinkenburg, *et al.* (E895 Collaboration), *Phys. Rev. Lett.* **83** (1999) 1295.
32. P. K. Sahu, W. Cassing, U. Mosel, A. Ohnishi, *Nucl. Phys. A* **672** (2000) 376.
33. P. Demorest, *et al.*, *Nature* **467** (2010) 1081.
34. J. Antoniadis, *et al.*, *Science* **340** (2013) 6131.
35. E. Fonseca *et al.*, arXiv:1603.00545 [astro-ph.HE].
36. M. Oertel, M. Hempel, T. Klähn and S. Typel, arXiv:1610.03361 [astro-ph.HE].
37. A. Akmal, V. R. Pandharipande, D. G. Ravenhall, *Phys. Rev. C* **58** (1998) 1804.
38. N.K. Glendenning, "Compact stars: Nuclear physics, particle physics, and general relativity", 2nd ed., Springer-Verlag, New York, 2000.
39. J. M. Lattimer, M. Prakash, *Astrophys. J.* **550** (2001) 42.
40. J. M. Lattimer and M. Prakash, *Science* **304** (2004) 536.
41. F. Weber, *Prog. Part. Nucl. Phys.* **54** (2005) 193.
42. I. Bombaci, arXiv:1601.05339 [nucl-th].
43. D. Chatterjee, I. Vidana, *Eur. Phys. J. A* **52** (2016) 29.
44. Y. Lim, C. H. Hyun, K. Kwak, C. H. Lee, *Int. J. Mod. Phys. E* **24** (2015) 12, 1550100.
45. H.-P. Duerr, *Phys. Rev.* **103** (1956) 469.
46. J.D. Walecka, *Annals Phys.* **83** (1974) 491.
47. J. Boguta, A. Bodmer, *Nucl. Phys. A* **292** (1977) 413.
48. B.D. Serot, J.D. Walecka, *Int. J. Mod. Phys. E* **6** (1997) 515.
49. J. Schaffner, I. N. Mishustin, *Phys. Rev. C* **53** (1996) 1416.
50. P. Papazoglou, *et al.*, *Phys. Rev. C* **59** (1999) 411.
51. S. Weissenborn, D. Chatterjee, J. Schaffner-Bielich, *Phys. Rev. C* **85** (2012) no.6, 065802 Erratum: [*Phys. Rev. C* **90** (2014) no.1, 019904]
52. C. Fuchs, H. Lenske, H. Wolter, *Phys. Rev. C* **52** (1995) 3043.
53. S. Typel, H. Wolter, *Nucl. Phys. A* **656** (1999) 331.

54. S. Typel, *Phys. Rev. C* **71** (2005) 064301.
55. C. M. Keil, F. Hofmann, H. Lenske, *Phys. Rev. C* **61** (2000) 064309.
56. F. Hofmann, C. M. Keil and H. Lenske, *Phys. Rev. C* **64** (2001) 025804.
57. I. Vidana, A. Polls, A. Ramos, M. Hjorth-Jensen and V. G. J. Stoks, *Phys. Rev. C* **61** (2000) 025802.
58. I. Vidana, A. Polls, A. Ramos, L. Engvik and M. Hjorth-Jensen, *Phys. Rev. C* **62** (2000) 035801.
59. T. Katayama and K. Saito, arXiv:1410.7166 [nucl-th].
60. K. Erkelenz, *Phys. Rept.* **13** (1974) 191.
61. R. Machleidt, K. Holinde, C. Elster, *Phys. Rept.* **149** (1987) 1.
62. Th.A. Rijken, V.G.J. Stoks, Y. Yamamoto, *Phys. Rev.* **59** (1999) 21.
63. Th.A. Rijken, *Phys. Rev. C* **73** (2006) 044007.
64. Th.A. Rijken, Y. Yamamoto, *Phys. Rev. C* **73** (2006) 044008.
65. Y. Yamamoto, T. Furumoto, N. Yasutake, Th.A. Rijken, *Phys. Rev. C* **90** (2014) 045805.
66. J. Haidenbauer, U.-G. Meissner, A. Nogga, H. Polinder, *Lect. Notes Phys.* **724** (2007) 113.
67. B. Holzenkamp, K. Holinde, J. Speth, *Nucl. Phys. A* **500** (1989) 485.
68. A. Reuber, K. Holinde, J. Speth, *Nucl. Phys. A* **570** (1994) 543.
69. Y. Fujiwara, C. Nakamoto, Y. Suzuki, *Phys. Rev.* **54** (1996) 2180.
70. M. Kohno, *et al.*, *Nucl. Phys. A* **674** (2000) 229.
71. Y. Fujiwara , Y. Suzuki , C. Nakamoto, *Prog. Part. Nucl. Phys.* **58** (2007) 439.
72. B. Borasoy, E. Epelbaum, H. Krebs, D. Lee, U.-G. Meissner, *Eur. Phys. J. A* **31** (2007) 105.
73. E. Epelbaum, H. Krebs, D. Lee, U.-G. Meissner, *Phys. Rev. Lett.* **106** (2011) 192501.
74. U.-G. Meissner, *Nucl. Phys. News* **24** (2014) 11.
75. E. Epelbaum, W. Gloeckle, U.-G. Meissner, *Nucl. Phys. A* **747** (2005) 362.
76. H. Polinder, J. Haidenbauer, U.-G. Meissner, *Nucl. Phys. A* **779** (2006) 244.
77. J. Haidenbauer, *et al.*, *Nucl. Phys. A* **915** (2013) 24.
78. S. Petschauer, *et al.*, *Eur. Phys. J. A* **52** (2016) 15.
79. A.K. Kerman, M.S. Weiss, *Phys. Rev. C* **8** (1973) 408.
80. L. Boltzmann, *Wien. Ber.* **66** (1872) 275.
81. E.A. Uehling, G.E. Uhlenbeck, *Phys. Rev.* **43** (1933) 552.
82. L.P. Kadanoff, G. Baym, "Quantum Statistical Mechanics", Benjamin, New York, 1962.
83. P. Danielewicz, *Ann. Phys.* **152** (1984) 239, 305.
84. G.F. Bertsch, S. Das Gupta, *Phys. Rep.* **160** (1988) 189.
85. W. Botermans, R. Malfliet, *Phys. Rep.* **198** (1990) 115.
86. S.R. de Groot, W.A. van Leeuwen, Ch.G. van Weert, "Relativistic Kinetic Theory", North-Holland, Amsterdam, 1980.
87. P. Danielewicz, R. Lacey, W. G. Lynch, *Science* **298** (2002) 1592.
88. C. Fuchs, H. Wolter, *Nucl. Phys. A* **589** (1995) 732.
89. T. Gaitanos, *et al.*, *Nucl. Phys. A* **732** (2004) 24.
90. B. Blaettel, V. Koch, U. Mosel, *Rept. Prog. Phys.* **56** (1993) 1.
91. S. Buss, *et al.*, *Phys. Rept.* **512** (2012) 1.
92. W. Ehehalt, W. Cassing, *Nucl. Phys. A* **602** (1996) 449.
93. W. Cassing, E.L. Bratkovskaya, *Phys. Rept.* **308** (1999) 65.
94. J. Aichelin, *Phys. Rept.* **202** (1991) 233.
95. C. Hartnack, *et al.*, *Eur. Phys. J.* **A1** (1998) 151.
96. S.W. Huang, *et al.*, *Prog. Part. Nucl. Phys.* **30** (1993) 105.

97. H. Sorge, H. Stöcker, W. Greiner, *Ann. Phys.* **192** (1989) 266.
98. T. Maruyama, *et al.*, *Nucl. Phys. A* **534** (1991) 720.
99. S. A. Bass, *et al.*, *Prog. Part. Nucl. Phys.* **41** (1998) 255 [*Prog. Part. Nucl. Phys.* **41** (1998) 225].
100. H. Feldmeier, *Nucl. Phys. A* **515** (1990) 147.
101. A. Ono, H. Horiuchi, T. Maruyama, A. Ohnishi, *Phys. Rev. Lett.* **68** (1992) 2898.
102. M.I. Nagy, T. Csörgő, *Int. J. Mod. Phys. A* **31** (2016) 1645017.
103. T. Gaitanos, H. Lenske, U. Mosel, *Phys. Lett. B* **675** (2009) 297.
104. T. Gaitanos, A. B. Larionov, H. Lenske, U. Mosel, *Nucl. Phys. A* **881** (2012) 240.
105. T. Gaitanos, H. Lenske, *Phys. Lett. B* **737** (2014) 256.
106. T. Gaitanos, C. Moustakidis, G. A. Lalazissis, H. Lenske, *Nucl. Phys. A* **954** (2016) 308.
107. H. Lenske, X. Cao, M. Dhar, T. Gaitanos, R. Shyam, arXiv:1603.00298 [nucl-th].
108. A. S. Botvina, *et al.*, arXiv:1608.05680 [nucl-th].
109. J. Steinheimer, A. S. Botvina, M. Bleicher, *J. Phys. Conf. Ser.* **668** (2016) no.1, 012007.
110. A. S. Botvina, *et al.*, *Phys. Lett. B* **742** (2015) 7.
111. J. Steinheimer, Z. Xu, P. Rau, C. Sturm, H. Stoecker, *Subnucl. Ser.* **48** (2013) 219.
112. A. S. Botvina, *et al.*, *Nucl. Phys. A* **881** (2012) 228.
113. A. S. Botvina, K. K. Gudima, J. Steinheimer, M. Bleicher, I. N. Mishustin, *Phys. Rev. C* **84** (2011) 064904.
114. C. Hartnack, A. Le Fevre, Y. Leifels, J. Aichelin, arXiv:1511.02646 [nucl-th].
115. A. Le Fevre, Y. Leifels, J. Aichelin, C. Hartnack, V. Kireyev and E. Bratkovskaya, *J. Phys. Conf. Ser.* **668** (2016) no.1, 012021.
116. A. Feliciello, T. Nagae, *Rep. Prog. Phys.* **78** (2015) 096301.
117. T.R. Saito, et al. (HypHI Collaboration), *Nucl. Phys. A* **954** (2016) 199.
118. C. Rappold, et al. (HypHI Collaboration), *Phys. Lett. B* **747** (2015) 129.
119. S. Nagamiya, *Prog. Theor. Exp. Phys.* **2012** (2012) 02B001.
120. The STAR collaboration, *Science 328*, 58 (2010).
121. B. Doenigus, *et al.* (ALICE collaboration), *Nucl. Phys. A* **547c** (2013) 904.
122. G. Agakishiev, *et al.*, arXiv:1310.6198.
123. I. Vassiliev for CBM collaboration. $http://indico2.riken.jp/indico/contributionListDisplay.py?confId = 2002$
124. NICA White Paper, $http://theor.jinr.ru/twiki-cgi/view/NICA/WebHome$; $http://nica.jinr.ru/files/BM@N$.
125. The PANDA collaboration, $http://www-panda.gsi.de$; and arXiv:physics/0701090.
126. J. Schwinger, *J. Math. Phys.* **2** (1961) 407.
127. L.V. Keldysh, *Zh. Eksp. Teor. Fiz.* **47** (1964) 1515.
128. K. Weber, *et al.*, *Nucl. Phys. A* **539** (1992) 713.
129. C.Y. Wong, *Phys. Rev. C* **25** (1982) 1460.
130. C. Gregoire, *et al.*, *Nucl. Phys. A* **465** (1987) 317.
131. K.A. Olive, *et al.* (Particle Data Group), *Chin. Phys. C*, **38** (2014) 090001.
132. T. Gaitanos, M. Kaskulov, *Nucl. Phys. A* **940** (2015) 181.
133. T. Gaitanos, M. M. Kaskulov, *Nucl. Phys. A* **899** (2013) 133.
134. A. B. Larionov, I. N. Mishustin, L. M. Satarov, W. Greiner, *Phys. Rev. C* **82** (2010) 024602.
135. A. B. Larionov, I. A. Pshenichnov, I. N. Mishustin, W. Greiner, *Phys. Rev. C* **80** (2009) 021601.
136. C. Fuchs, P. Essler, T. Gaitanos, H. H. Wolter, *Nucl. Phys. A* **626** (1997) 987.

137. J. Rizzo, P. Chomaz, M. Colonna, *Nucl. Phys. A* **806** (2008) 40.
138. V. Baran, M. Colonna, V. Greco, M. Di Toro, *Phys. Rept.* **410** (2005) 335.
139. S. Typel, *et al.*, *Phys. Rev. C* **81** (2010) 015803.
140. A.S. Botvina, *et al.*, *Nucl. Phys. A* **475** (1987) 663.
141. J.P. Bondorf, *et al.*, *Phys. Rept.* **257** (1995) 133.
142. R. Ogul, *et al.*, *EPJ Web Conf.* **93** (2015) 02022.
143. R. Ogul, *et al.*, *Acta Physica Polonica B Proceedings Supplement* **8** (2015) 645.
144. H. Imal, *et al.*, *Phys. Rev. B* **91** (2015) no.3, 034605.
145. T. Gaitanos, A. B. Larionov, H. Lenske, U. Mosel, *Phys. Rev. C* **81** (2010) 054316.
146. M. Lisa, *et al.* (EOS collaboration), *Phys. Rev. Lett.* **75** (1995) 2662.
147. W. Reisdorf, *et al.* (FOPI Collaboration), *Nucl. Phys. A* **612** (1997) 493.
148. J. Benlliure, *et al.*, *Nucl. Phys. A* **683** (2001) 513.
149. F. Rejmund, *et al.*, *Nucl. Phys. A* **683** (2001) 540.
150. T. Gaitanos, H. Lenske, U. Mosel, *Phys. Lett. B* **663** (2008) 197.
151. S. Leray, *et al.*, *Phys. Rev. C* **65** (2002) 044621.
152. D. Henzlova, *et al.*, *Phys. Rec. C* **78** (2008) 044616.
153. A. B. Larionov, T. Gaitanos, U. Mosel, *Phys. Rev. C* **85** (2012) 024614.
154. A.B. Kaidalov, P.E. Volkovitsky, *Z. Phys. C* **63** (1994) 517.
155. J.J. de Swart, T.A. Rijken, P.M. Maessen, R.G.E. Timmermans, *Nuovo Cimento A* **102** (1989) 203.
156. Th.A. Rijken, Y. Yamamoto, [arXiv:nucl-th/0608074].
157. Y. Fujiwara, *et al.*, **Phys. Rev. C 64** (2001) 054001.